

# Electronic structure changes during the surface-assisted formation of a graphene nanoribbon

Christopher Bronner,<sup>1,2,a)</sup> Manuel Utecht,<sup>3</sup> Anton Haase,<sup>2</sup> Peter Saalfrank,<sup>3</sup>  
Tillmann Klamroth,<sup>3</sup> and Petra Tegeder<sup>1,2</sup>

<sup>1</sup>Ruprecht-Karls-Universität Heidelberg, Physikalisch-Chemisches Institut, Im Neuenheimer Feld 253, 69120 Heidelberg, Germany

<sup>2</sup>Freie Universität Berlin, Fachbereich Physik, Arnimallee 14, 14195 Berlin, Germany

<sup>3</sup>Universität Potsdam, Institut für Chemie, Theoretische Chemie, Karl-Liebknecht-Straße 24-25, 14476 Potsdam, Germany

(Received 18 June 2013; accepted 13 December 2013; published online 8 January 2014)

High conductivity and a tunability of the band gap make quasi-one-dimensional graphene nanoribbons (GNRs) highly interesting materials for the use in field effect transistors. Especially bottom-up fabricated GNRs possess well-defined edges which is important for the electronic structure and accordingly the band gap. In this study we investigate the formation of a sub-nanometer wide armchair GNR generated on a Au(111) surface. The on-surface synthesis is thermally activated and involves an intermediate non-aromatic polymer in which the molecular precursor forms polyanthrylene chains. Employing angle-resolved two-photon photoemission in combination with density functional theory calculations we find that the polymer exhibits two dispersing states which we attribute to the valence and the conduction band, respectively. While the band gap of the non-aromatic polymer obtained in this way is relatively large, namely  $5.25 \pm 0.06$  eV, the gap of the corresponding aromatic GNR is strongly reduced which we attribute to the different degree of electron delocalization in the two systems. © 2014 AIP Publishing LLC. [<http://dx.doi.org/10.1063/1.4858855>]

## I. INTRODUCTION

While the continuous down-scaling of microelectronics has been successfully applied in the past decades yielding faster, smaller, and more energy efficient devices, this method is steadily approaching fundamental physical limits which are an inevitable consequence of the miniaturization.<sup>1,2</sup> In recent years, efforts to overcome these limits by changing the semiconducting material have dealt intensively with carbon-based systems such as graphene<sup>3–7</sup> or carbon nanotubes.<sup>8,9</sup> While graphene exhibits an enormous charge carrier mobility it has no technologically relevant band gap. Furthermore, in any realization of graphene-based devices, its infinite two-dimensional nature cannot be maintained, particularly in nanoscale structures where lateral confinement significantly alters the electronic properties.

Instead of dealing with lateral constrictions as a problem, incorporating edges into the very principle of graphene structures leads to the concept of graphene nanoribbons (GNRs) which are quasi-one dimensional, narrow and flat stripes of graphene, and additionally possess a band gap.<sup>10,11</sup> Numerous theoretical<sup>12–21</sup> as well as experimental<sup>22–27</sup> studies have shown that this band gap depends on the GNR type, i.e., on its width as well as on the shape of its edges, e.g., zigzag or armchair, much like in carbon nanotubes. While the inverse power law for the width dependence of the band gap is found to be universal in nanoribbons of several tens of nanometers width,<sup>22</sup> the influence of the GNR's chiral vector becomes more and more important as the ribbons become as narrow

as a few carbon atoms.<sup>17</sup> GNRs thus provide a whole variety of electronic structures with different band gaps and dispersions along the ribbon axis. Since the band structure is of fundamental importance for the functionality of nanoelectronic devices, this is a big advantage for technological application but on the other hand it requires a high degree of precision in the fabrication process.

Conventional top-down approaches for GNR fabrication, such as lithography<sup>22</sup> or unzipping of carbon nanotubes,<sup>24</sup> cannot provide defect-free edges and narrow ribbons.

Generally, in the fabrication of nanostructures, on-surface synthesis<sup>28</sup> is a powerful alternative to the aforementioned top-down approaches and has been successfully applied for GNR assembly by Cai *et al.*<sup>25</sup> However, this concept is limited by the availability of suitable precursor molecules.

In the aforementioned work, the authors introduce a monomer which is substituted by bromine. Deposited onto a Au(111) surface, these molecules are activated by detachment of bromine and polymerize after heating to 470 K and, in a second step, undergo a cyclodehydrogenation at 670 K yielding defect-free armchair GNRs with a well-defined width (see Fig. 1). The gold surface (chosen for its inertness) plays an important catalytic role in the dehydrogenation step of this bottom-up reaction.<sup>29</sup>

While the electronic structure of the GNR has been studied recently,<sup>30–33</sup> with the present paper we want to contribute insight into the band structure of narrow graphene nanoribbons by looking at the intermediate step of the surface-assisted reaction pathway, i.e., the polyanthrylene chains which occur after the first heating step. Using two-photon photoemission and density functional theory (DFT) we find

<sup>a)</sup>Electronic mail: bronner@uni-heidelberg.de

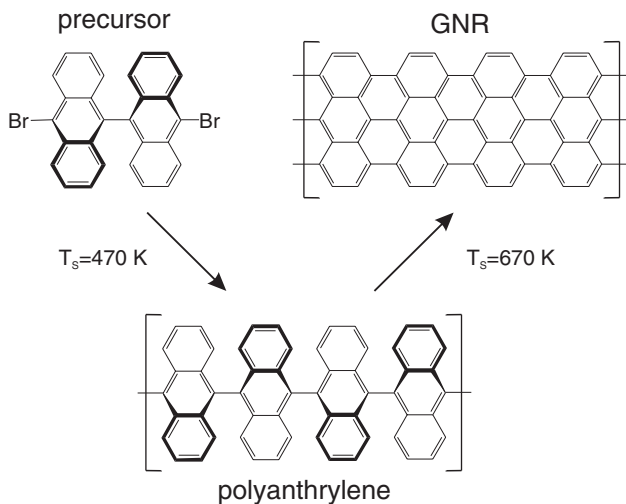


FIG. 1. Surface-assisted bottom-up formation of the armchair nanoribbon *via* the intermediate non-aromatic polyanthrylene. The polymerization is induced by heating the sample to 470 K. Cyclodehydrogenation leads to the formation of an aromatic GNR at 670 K.

that the band gap of the intermediate polymer is by a factor of two larger than the one in the GNR because the nature of the electronic system is fundamentally different, i.e., the band gap of the GNR is predominantly a result of the aromatic, delocalized  $\pi$ -system which is not present in the polymer.

## II. METHODS

We employed angle-resolved two-photon photoemission (AR-2PPE) for the investigation of the band structure because it allows the study of both occupied and unoccupied electronic states as well as their dispersion.<sup>34–42</sup> In this surface-sensitive pump-probe method, electrons are excited in a two-step process by laser pulses of photon energy  $h\nu$  which is smaller than the work function  $\Phi$ . Unoccupied electronic states above the Fermi level  $E_F$  are populated by the pump pulse, subsequently photoelectrons are ejected from these states by the probe pulse. The kinetic energy  $E_{\text{kin}}$  of the emitted electrons is measured in a time-of-flight (TOF) spectrometer. In the studies presented here, pump and probe pulse have the same photon energy which is referred to as one-color 2PPE (1C-2PPE). Occupied states are investigated in a two-photon process *via* a virtual intermediate state or through resonant excitation of an unoccupied state. In order to determine whether an electronic state is occupied or unoccupied, the change in kinetic energy of the corresponding peak in the 2PPE spectrum is observed while varying the photon energy. Whereas a feature originating from an unoccupied state will shift by an energy equal to the photon energy change, the peak of an occupied state changes in energy twice as much due to the involved two-photon process.<sup>43</sup> 2PPE spectra are usually displayed as a function of final state energy with respect to the Fermi level,  $E_{\text{Final}} - E_F = E_{\text{kin}} + \Phi$ . This is a convenient quantity for determining the binding energy with respect to  $E_F$ , since this is done simply by subtracting  $h\nu$  once (unoccupied state) or twice (occupied state) from  $E_{\text{Final}}$ . In order to measure the dispersion of occupied and unoccupied states as

a function of the momentum parallel to the surface,

$$k_{\parallel} = \sqrt{\frac{2m_e E_{\text{kin}}}{\hbar^2}} \cdot \sin \vartheta, \quad (1)$$

we rotated the sample in front of the TOF analyzer. Therein,  $\vartheta$  denotes the angle between the surface normal and the emission angle. The effective mass  $m_{\text{eff}}$  in the region around the  $\bar{\Gamma}$  point ( $k_{\parallel} = 0$ ) can be determined by fitting a parabola corresponding to the behavior of a quasi-free electron:

$$E(k_{\parallel}) = E_0 + \frac{\hbar^2 k_{\parallel}^2}{2m_{\text{eff}}}. \quad (2)$$

Femtosecond laser pulses were generated in a Ti:Sapphire laser system which is equipped with an optical parametric amplifier (OPA) providing pulses with tunable wavelengths ranging over most of the visible spectrum. This OPA output was frequency-doubled in a  $\beta$ -barium-borate (BBO) crystal yielding pulses in the ultraviolet region. The laser beam was p-polarized and directed onto the sample at an angle of  $45^\circ$  with respect to the spectrometer axis and the surface normal (if  $\vartheta = 0$ ).

All measurements were performed in an ultrahigh vacuum chamber (base pressure  $1 \times 10^{-10}$  mbar) in which the Au(111) single crystal was mounted. A flow cryostat operated with liquid nitrogen and equipped with resistive heating enabled us to control the sample temperature from 90 K to more than 800 K. Routine cycles of  $\text{Ar}^+$  sputtering and annealing were performed to clean the surface. Subsequently, the precursor molecules were evaporated from a Knudsen cell evaporator (held at 450 K) onto the surface (kept at 300 K). The sample was characterized by means of temperature programmed desorption (TPD) of molecules from the multilayer and detached bromine atoms from the first layer using a quadrupole mass spectrometer (QMS) which ensures a sub-monolayer coverage. TPD curves were recorded while ramping the sample temperature to 470 K, at which the polymerization occurs (the temperature was kept constant for 10 min). All 2PPE measurements were conducted at 90 K.

A detailed discussion of the geometrical structure of both the intermediate polymer as well as the GNR have been given in a previous paper.<sup>30</sup> There, high-resolution electron energy loss spectroscopy (HREELS) is employed to demonstrate the formation of a three-dimensional polyanthrylene upon the first heating step and the GNR formation in the second step. HREELS has proven to be a reliable surface-sensitive technique and has been successfully applied to characterize GNRs in the past.<sup>30,44</sup> Furthermore, in the cited paper we show that Xe co-adsorption experiments reveal the coverage to lie around  $2/3$  of a monolayer. Since we employ the same preparation method as Cai *et al.*<sup>25</sup> it is reasonable to assume that the GNRs formed in our experiments exhibit a similar distribution of the chain length as well as an isotropic distribution of the chain orientations within the surface plane. The latter phenomenon has been discussed with respect to its consequences for angle-resolved experiments in our previous study.<sup>30</sup> In an angle-resolved experiment, both the momentum component parallel to the ribbon  $k_{\parallel}$  as well as perpendicular to it  $k_{\perp}$  have to be taken into account. Therefore, the momentum detected

in our experiment will in general be higher than  $k_{\parallel}$  which leads to a smearing of the signal to higher  $k_{\parallel}$ , but not in binding energy. This should be kept in mind when discussing the effective mass of a delocalized electronic state.

The theoretical calculations were performed using density functional theory with the Gaussian 09 program package.<sup>45</sup> As in the investigations for GNR,<sup>30</sup> we used different functionals, i.e., PBE0<sup>46</sup> and CAM-B3LYP<sup>47</sup> with a 6-311G\*\* basis set, for the density functional calculations. We get qualitatively the same trends and results for the different functionals, however, quantitatively large differences are found, for instance for the band gap. The same observation was made in Ref. 30. There, it seemed and was stated that CAM-B3LYP performed better for the band gap of GNR than PBE0. However, given the new interpretation of the experimental results, which leads to a band gap of about 2.6 eV (see Sec. IV), PBE0 is much better than CAM-B3LYP (2.7 eV gap for PBE0 compared to 4.35 eV gap for CAM-B3LYP<sup>30</sup>). For the present system surprisingly CAM-B3LYP fits quantitatively much better to experiment than PBE0. Nevertheless, both show the same trends and agree qualitatively. Band structures, band gaps, and density of states (DOS) were calculated for the infinite polymer and for finite oligomers, respectively. The oligomers were saturated with hydrogen atoms at the ends. We used a grid of 120 k-points for the first Brillouin zone and a cutoff of 600 bohr in real space for the periodic calculations. The unit cell consists of two anthrylene units in all cases. All geometries were fully optimized without taking the gold surface into account. Structures with twisted anthrylene units were optimized, keeping the twist angle fixed (see below). DOS plots were achieved by Lorentzian broadening of the Kohn-Sham orbital energies for the finite oligomers or the crystal orbital energies  $\epsilon_i$  in the first Brillouin zone for the finite polymers with a broadening factor  $\Gamma = 0.2\text{eV}$ :

$$D(\epsilon) = \sum_i \frac{1}{\pi} \frac{\frac{1}{2}\Gamma}{(\epsilon - \epsilon_i)^2 + (\frac{1}{2}\Gamma)^2}. \quad (3)$$

### III. RESULTS AND DISCUSSION

A series of one-color 2PPE spectra recorded with different photon energies in the ultraviolet regime is shown in Fig. 2. The series has been measured after annealing the precursor-covered surface to 470 K, thus in the polymeric phase. Besides known features of the gold substrate, namely two prominent peaks assigned to the  $d$ -bands (not shown here), two states are observed which are induced by the adsorbate. The corresponding peaks are observed close to the Fermi edges of the spectra and their energetic shift with varying photon energy is shown in the inset of Fig. 2. The valence band (VB) peak exhibits a slope of more than two which would not be expected in a one-color 2PPE experiment. However, the peak position at the highest photon energy which deviates from the trend observed for the remaining spectra is most likely shifted to higher final state energies due to a partially resonant excitation via the other observed state which is unoccupied (see below). From the respective slopes, we can conclude that the peak at lower energies (la-

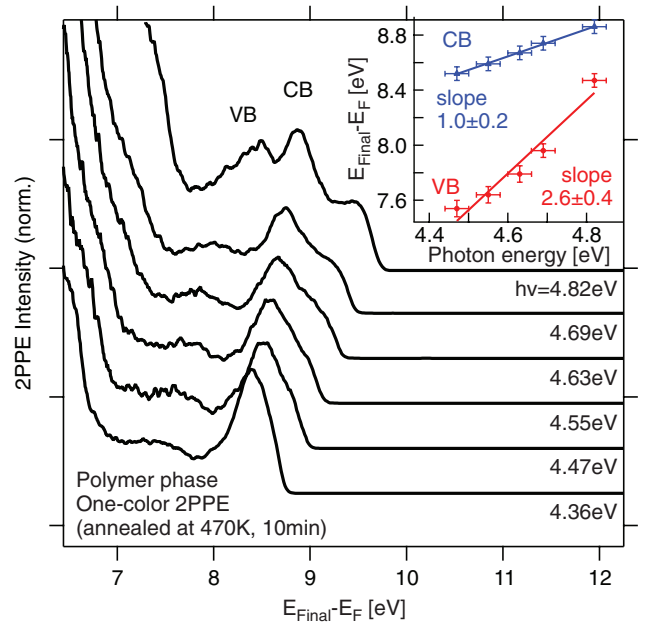


FIG. 2. One-color 2PPE spectra of the polymer phase for different photon energies. The spectra were normalized with respect to a spectral feature arising from the gold  $d$ -bands. Two peaks are found close to the Fermi edge on the high energy side of the spectrum. From the shift of the peak positions as a function of photon energy (inset) we identify one as unoccupied and the other one as occupied. We assign them to the valence band (VB) and conduction band (CB), respectively.

beled “VB”) originates from an occupied electronic state located at  $E_{\text{VB}} = -1.18 \pm 0.04\text{eV}$  with respect to the Fermi level of the gold substrate while the high energy peak (“CB”) corresponds to an unoccupied state at  $E_{\text{CB}} = 4.07 \pm 0.04\text{eV}$ . This yields a band gap of  $\Delta = 5.25 \pm 0.06\text{eV}$ . Furthermore, the low energy cutoff in these 2PPE spectra (not shown in the figure) yields the work function of the polymer-covered surface to be  $\Phi = 4.81 \pm 0.01\text{eV}$ . Note that based on xenon co-adsorption and TPD experiments we infer a polymer coverage of approximately 2/3 monolayer.<sup>30</sup>

Having determined the energetic position of the electronic states which arise upon formation of the polyanthrylene chains, we now used angle-resolved 2PPE to measure the dispersion of these states, i.e., the degree of charge carrier localization or delocalization parallel to the surface. As seen in Fig. 3, both states show a parabolic dispersion around the  $\Gamma$ -point. While the unoccupied state exhibits a dispersion typical for quasi-free electrons, the occupied state shows a hole-like dispersion with decreasing energy at higher  $k_{\parallel}$ . Note that the dispersion curve of the conduction band (CB) is plotted with respect to the left energy axis and the dispersion of the valence band accordingly to the one on the right. As indicated in the figure we fitted a parabola according to Eq. (2). The behavior of the unoccupied electronic state is well described by an effective mass of  $m^* = 1.35 \pm 0.07$ . The absolute value of the corresponding effective mass for the occupied state is the same, namely  $m^* = -1.37 \pm 0.15$ . Thus, both states show a behavior similar to quasi-free charge carriers. However, this only holds true for small  $k_{\parallel}$ , whereas the dispersion significantly differs from a parabola at higher parallel momenta.

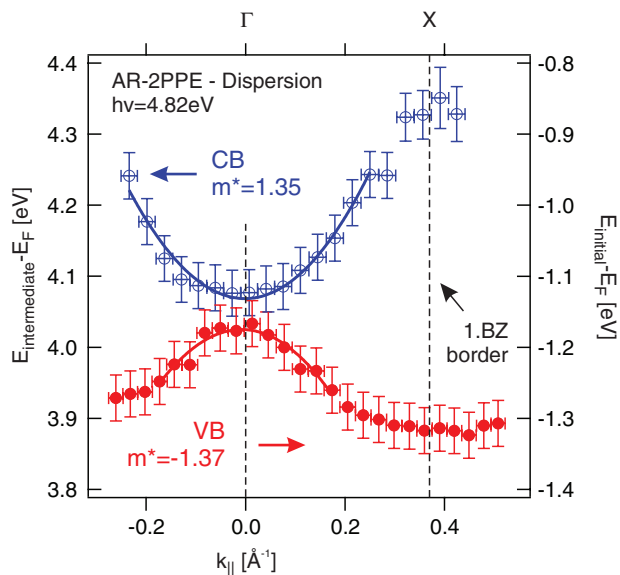


FIG. 3. Dispersion of valence band (VB) and conduction band (CB) around the  $\Gamma$  point. The valence band is shown with its initial binding energy  $E_{\text{initial}}$  (right axis), the conduction band is displayed with the intermediate state energy  $E_{\text{intermediate}}$  corresponding to the binding energy of this band. Parabolic fits yield the effective masses of both bands around the  $\Gamma$  point. The border of the first Brillouin zone (BZ) is marked.

Based on scanning tunneling microscopy (STM) measurements of the periodicity of the polyanthrylene chain,<sup>25</sup> we calculated the boundary of the first Brillouin zone which is shown in Fig. 3. While we cannot access higher  $k_{\parallel}$  in our experiment, it seems that indeed the dispersion curves reach a turning point at the Brillouin zone boundary.

We performed DFT calculations to be able to bring our experimental findings into the context of the whole one-dimensional band structure. Both an infinite polyanthrylene chain with periodic boundary conditions and oligomers of two, four, and six anthrylene units, respectively, were investigated. In the free polyanthrylene without an underlying substrate, the dihedral angle between adjacent anthrylene units is  $90^\circ$ . However, due to the attractive interaction with the metal substrate, e.g., *via* dispersive forces, the dihedral angle is expected to be altered at the surface, presumably to be lowered in the sense that the whole polyanthrylene is pulled toward the surface. Furthermore, surface polarization effects will lower the band gaps with respect to our gas phase calculations as explained in detail by Ruffieux *et al.*<sup>32</sup> We performed DFT studies at various dihedral angles between  $30^\circ$  and  $90^\circ$  for the free molecule to account for the distorted geometry at the surface.

We calculated the electronic DOS for the three oligomers and the polymer, each with dihedral angles of  $30^\circ$ ,  $45^\circ$ ,  $60^\circ$ , and for the fully optimized geometry ( $90^\circ$ ). Figure 4 shows exemplarily the DOS for a dihedral angle of  $45^\circ$ . In all three cases a gap of about 5 eV is found between the occupied (black) and unoccupied (red) states, largely independent of oligomer size. While only the band gap changes quantitatively with varying dihedral angle, for no geometrical configuration or chain length an end state similar to the one which occurs in the center of the band gap of a finite ar-

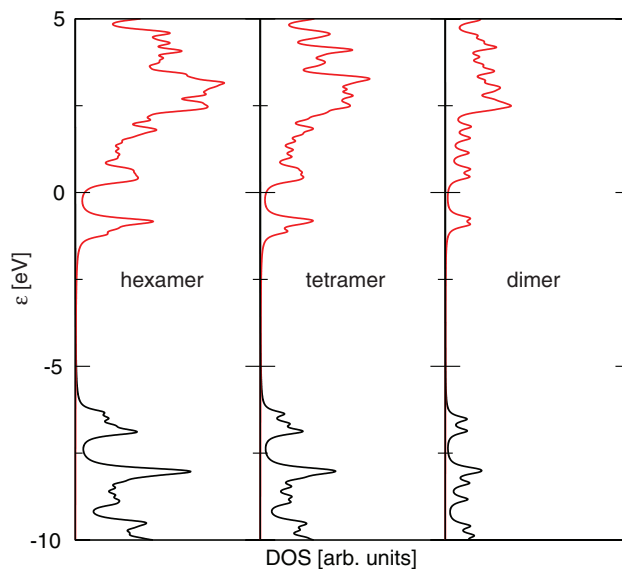


FIG. 4. Density of states calculated with the CAM-B3LYP functional for three different oligomers with two, four, and six anthrylene units. Unoccupied and occupied orbitals are displayed in red and black, respectively. A large band gap is observed but no end state lying in this gap. The dihedral angle was fixed as  $45^\circ$  (see text).

omatic GNR<sup>30,48,49</sup> is found. The CAM-B3LYP calculations deliver band gaps which are very close to experimental values while PBE0 clearly underestimates the gaps by about 1.4 eV. The GNRs (and therefore the polyanthrylene chains) produced in our experiments are assumed to be of dozens of units in length.<sup>30</sup> Their band structure therefore resembles the one calculated with periodic boundary conditions. The lattice constants for all four angles correspond very well to the experimental value. Note that the DOS of the infinite GNR (periodic boundary conditions) and the finite oligomers show only minor differences.

Figure 5 shows the band structure calculated with the CAM-B3LYP functional for a dihedral angle of  $45^\circ$ . A large direct band gap is found between valence and conduction bands, which exhibit a different dispersion in the regime

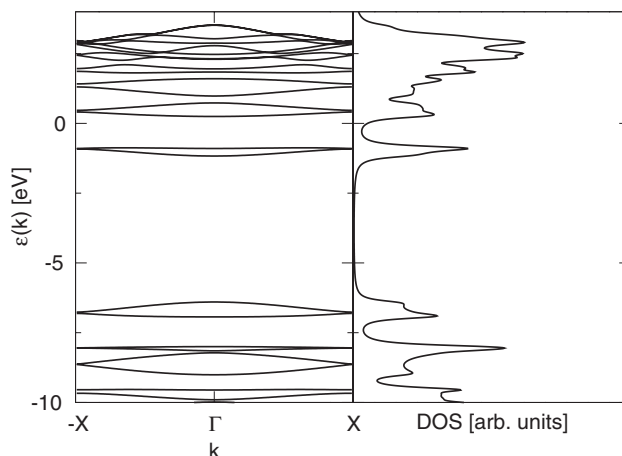


FIG. 5. Band structure and density of states (DOS) calculated at a dihedral angle of  $45^\circ$  and for periodic boundary conditions. The X point corresponds to a parallel momentum of  $0.36 \text{ \AA}^{-1}$ .

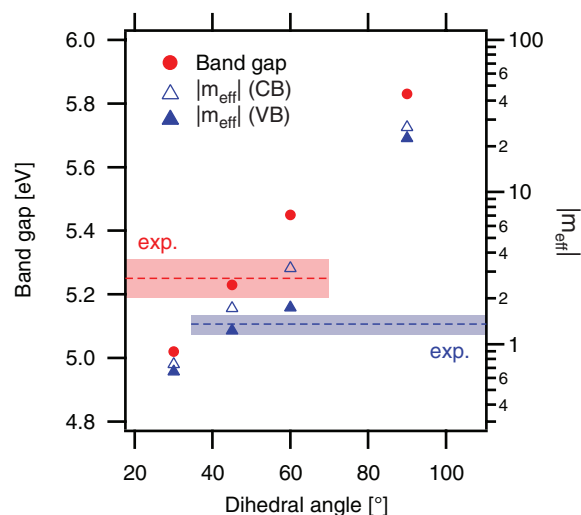


FIG. 6. Calculated band gap for periodic boundary conditions (using CAM-B3LYP) and the absolute value of the effective masses  $m_{\text{eff}}$  of valence and conduction bands, respectively, as a function of the dihedral angle. For comparison, the experimental values are marked with a dashed line. The shaded areas indicate the experimental error.

around the  $\Gamma$  point where a parabolic approximation is valid. The values for band gap and effective masses calculated with CAM-B3LYP are plotted in Fig. 6 as a function of the dihedral angle, together with the experimental values. A continuous linear increase of the band gap is observed with increasing angle while both effective masses (or their absolute value) rise exponentially but in a similar fashion for valence and conduction bands. In Table I, the band gaps and the effective masses of the polyanthrylene at various dihedral angles are compared for the two functionals employed. Band gaps calculated with PBE0 are significantly lower (about 2 eV) than those for CAM-B3LYP while the dispersion is rather independent of the functional. At  $45^\circ$  the calculated values (using CAM-B3LYP) fit best to those determined in 2PPE. Note however, that a comparison between the theoretical calculations and the experimental results cannot be used to determine the dihedral angle, for example because the interaction with the substrate which is not taken into account in our calculations should significantly influence the adsorption geometry and thus the dihedral angle as well as band gaps. As already

TABLE I. Comparison of the calculated band gaps and the effective masses of the valence band  $m_{\text{VB}}^*$  and the conduction band  $m_{\text{CB}}^*$ , respectively, of the polyanthrylene using two different functionals CAM-B3LYP and PBE0.

Dihedral angle	Band gap (eV)	$m_{\text{VB}}^*$	$m_{\text{CB}}^*$
CAM-B3LYP			
$30^\circ$	5.02	-0.66	0.74
$45^\circ$	5.23	-1.23	1.72
$60^\circ$	5.45	-1.74	3.15
$90^\circ$	5.83	-22.59	-26.63
PBE0			
$30^\circ$	3.03	-0.69	0.75
$45^\circ$	3.22	-0.90	1.13
$60^\circ$	3.42	-1.47	2.41
$90^\circ$	3.77	-23.82	-28.82

explained above, surface interaction will also lower the band gaps compared to our gas phase results.<sup>32</sup> The calculated band gap for a dihedral angle of  $45^\circ$  is 5.23 eV, the effective masses for valence and conduction bands amount to -1.23 and 1.72, respectively. The strong increase of both effective masses with increasing dihedral angle indicates that there is a higher electronic interaction between the anthracene units at lower angles while a perpendicular shape more or less inhibits the interaction. We therefore conclude that electron transport along the polyanthrylene chain can predominantly be attributed to the  $\pi$  electrons of the aromatic anthrylene units once they interact with those of the adjacent monomer. Considering the above results from experiment as well as from DFT calculations, we assign the unoccupied state, which was found in 2PPE, to the conduction band of the polymer and the occupied state to the valence band. With the above found energetic positions, we conclude that the polyanthrylene exhibits a direct band gap of  $\Delta = 5.25 \pm 0.06$  eV.

#### IV. COMPARISON OF THE BAND STRUCTURE: POLYMER VS. NANORIBBON

Looking at the differences of the intermediate polyanthrylene investigated in the present work and the product of the surface-assisted chemical reaction, the nanoribbon,<sup>30</sup> we can gain insight into the different stages of the electronic band structure in the formation process of narrow graphene nanoribbons. In a previous study, we have reported on the electronic structure of the aromatic GNR.<sup>30</sup> There, we found a dispersing state lying 3.92 eV above the Fermi level as well as another localized state at 1.44 eV with respect to the Fermi energy. Due to the localization of the lower lying state and considering the results of our DFT calculations, we concluded that the lower lying state is an end state localized at the short ends of the GNR while the dispersing, higher-lying state was the conduction band. From this interpretation we concluded that the band gap was 5.1 eV. In the meantime, scanning tunneling microscopy and scanning tunneling spectroscopy (STS) experiments<sup>48,49</sup> have confirmed the lower lying state at 1.44 eV but have also revealed a very weak feature in STS close to the Fermi level at 30 meV. Based on the spatial distribution of the state close to the Fermi level, this feature has been assigned to Tamm states which can be thought of as one-dimensional surface states of the two-dimensional GNR structure.<sup>48,49</sup> We believe that these Tamm states are in fact identical to what we interpreted as end states in our previous study. We furthermore conclude, based on the spatial distribution observed in STM, that while we are unable to observe the end state close to the Fermi level due to its weak intensity, the peak which we observe at 1.44 eV corresponds to the conduction band of the GNR. This interpretation fits to the measured conductance spectra<sup>48</sup> and as a result, we observe a band gap of the GNR which amounts to 2.60 eV. The state at 3.92 eV which was previously assigned to the conduction band could therefore originate from a higher lying band or from an image potential state. Fig. 7 shows a comparison of the energetic positions of the valence and conduction bands for the polymer and the GNR, respectively. The band gap is reduced from 5.25 eV in the

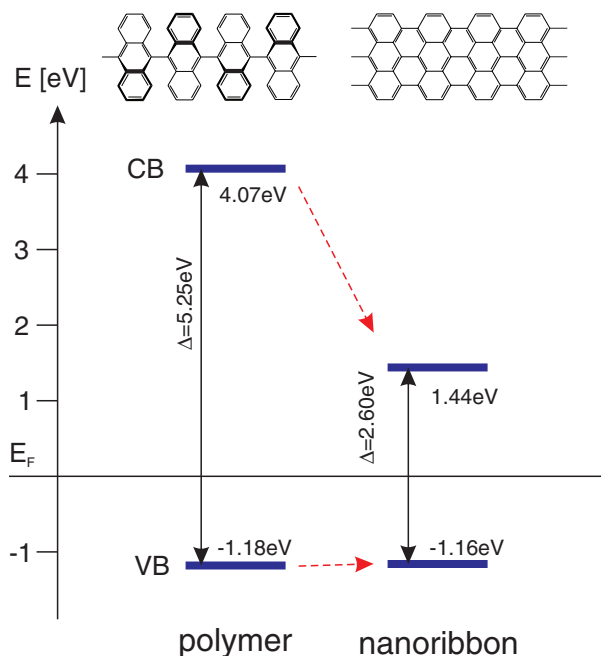


FIG. 7. Comparison of the electronic structure of the non-aromatic polymer with the one of the corresponding aromatic graphene nanoribbon.<sup>30</sup> The band gap is reduced and the conduction band is shifted to lower energies.

polymer case to 2.60 eV for the GNR which corresponds to a reduction by about 50%. Besides this decrease in magnitude, the position of the band gap with respect to the Fermi level of the metal substrate is shifted to lower energies. While the different geometries of the two structures which is mainly due to different dihedral angles certainly affects the band gap, the extrapolation of the data for the band gap presented in Fig. 6 to an angle of  $0^\circ$ , i.e., a flat structure, suggest that the gap should not be reduced by around 2.5 eV due to the altered dihedral angle alone. Instead, the drastically reduced band gap is an effect of the extended delocalized  $\pi$ -system of the aromatic GNR, similar to graphene. In this planar configuration, the electron mobility is strongly increased and therefore the electronic structure resembles much more the one of graphene with its Dirac cones than the electronic structure derived from hybridizing molecular orbitals of the neighboring anthracene units which lead to the bands observed in the polymer. The overall down-shift of the band structure with respect to the Fermi level is most likely due to the increased hybridization of the GNR bands with the metal bands and a corresponding partial charge transfer. Another difference between the polymer and the GNR which is observed at least in theory is the absence of an end state in case of the polymer. This difference is an indication that the formation of end states requires the extended two-dimensional electron gas which is present only in the GNR.

## V. CONCLUSION

We employed two-photon photoemission and density functional theory to study the band structure of a polyanthrylene in order to follow the substrate-mediated chemical formation of a sub-nanometer wide armchair nanoribbon

on the Au(111) surface. We determined the valence band to be located at  $E_{VB} = -1.18$  eV and the conduction band at  $E_{CB} = 4.07$  eV with respect to the Fermi level. The very formation of bands in the non-aromatic polymer which exhibits only  $\sigma$  bonds between the anthracene monomers is noticeable. However, our calculations demonstrate that while in the fully optimized geometry, with perpendicular anthrylene units, the valence and conduction bands disperse only weakly, their effective mass is significantly lowered as the twisting angle between the monomers is reduced to account for the geometry of adsorbed polyanthrylene. A fundamental difference between the two systems is the occurrence of an electronic state localized at the ends of the one-dimensional structure, which in contrast to the GNR is not observed in the polyanthrylene. Compared to the intermediate polymer, the band gap of the GNR as the final reaction product is strongly reduced due to the different nature of the electronic structure of the GNR with its extended delocalized  $\pi$ -system which resembles a two-dimensional electron gas. Additionally, the electronic structure of the GNR is lowered in energy relative to the metal band structure due to a higher degree of hybridization between GNR and metal bands.

## ACKNOWLEDGMENTS

We gratefully acknowledge financial support by the Focus Area NanoScale at the Freie Universität Berlin and the German Research Foundation (DFG) through collaborative research center SFB 658.

- <sup>1</sup>M. Schulz, *Nature* **399**, 729 (1999).
- <sup>2</sup>R. Chau, B. Doyle, S. Datta, J. Kavalieros, and K. Zhang, *Nature Mater.* **6**, 810 (2007).
- <sup>3</sup>A. K. Geim and K. S. Novoselov, *Nature Mater.* **6**, 183 (2007).
- <sup>4</sup>K. S. Novoselov, A. K. Geim, S. V. Morozov, D. Jiang, Y. Zhang, S. V. Dubonos, I. V. Grigorieva, and A. A. Firsov, *Science* **306**, 666 (2004).
- <sup>5</sup>K. S. Novoselov, A. K. Geim, S. V. Morozov, D. Jiang, M. I. Katsnelson, I. V. Grigorieva, S. V. Dubonos, and A. A. Firsov, *Nature* **438**, 197 (2005).
- <sup>6</sup>I. Meric, M. Y. Han, A. F. Young, B. Ozyilmaz, P. Kim, and K. L. Shepard, *Nat. Nanotechnol.* **3**, 654 (2008).
- <sup>7</sup>F. Xia, D. Farmer, Y.-M. Lin, and P. Avouris, *Nano Lett.* **10**, 715 (2010).
- <sup>8</sup>S. J. Tans, A. R. M. Verschueren, and C. Dekker, *Nature* **393**, 49 (1998).
- <sup>9</sup>A. Javey, J. Guo, Q. Wang, M. Lundstrom, and H. Dai, *Nature* **424**, 654 (2003).
- <sup>10</sup>S. Dutta and S. K. Pati, *J. Mater Chem.* **20**, 8207 (2010).
- <sup>11</sup>H. Terrones, R. Lv, M. Terrones, and M. S. Dresselhaus, *Rep. Prog. Phys.* **75**, 062501 (2012).
- <sup>12</sup>K. Nakada, M. Fujita, G. Dresselhaus, and M. S. Dresselhaus, *Phys. Rev. B* **54**, 17954 (1996).
- <sup>13</sup>M. Fujita, K. Wakabayashi, K. Nakada, and K. Kusakabe, *J. Phys. Soc. Jpn.* **65**, 1920 (1996).
- <sup>14</sup>V. Barone, O. Hod, and G. E. Scuseria, *Nano Lett.* **6**, 2748 (2006).
- <sup>15</sup>M. Ezawa, *Phys. Rev. B* **73**, 045432 (2006).
- <sup>16</sup>Y.-W. Son, M. L. Cohen, and S. G. Louie, *Nature* **444**, 347 (2006).
- <sup>17</sup>Y.-W. Son, M. L. Cohen, and S. G. Louie, *Phys. Rev. Lett.* **97**, 216803 (2006).
- <sup>18</sup>L. Yang, C.-H. Park, Y.-W. Son, M. L. Cohen, and S. G. Louie, *Phys. Rev. Lett.* **99**, 186801 (2007).
- <sup>19</sup>H. Zheng, Z. F. Wang, T. Luo, Q. W. Shi, and J. Chen, *Phys. Rev. B* **75**, 165414 (2007).
- <sup>20</sup>A. J. Chaves, G. D. Lima, W. de Paula, C. E. Cordeiro, A. Delfino, T. Frederico, and O. Oliveira, *Phys. Rev. B* **83**, 153405 (2011).
- <sup>21</sup>H. Feldner, Z. Y. Meng, T. C. Lang, F. F. Assaad, S. Wessel, and A. Honecker, *Phys. Rev. Lett.* **106**, 226401 (2011).
- <sup>22</sup>M. Y. Han, B. Özyilmaz, Y. Zhang, and P. Kim, *Phys. Rev. Lett.* **98**, 206805 (2007).

- <sup>23</sup>X. Li, X. Wang, L. Zhang, S. Lee, and H. Dai, *Science* **319**, 1229 (2008).
- <sup>24</sup>D. V. Kosynkin, A. L. Higginbotham, A. Sinitskii, J. R. Lomeda, A. Dimiev, B. K. Price, and J. M. Tour, *Nature* **458**, 872 (2009).
- <sup>25</sup>J. Cai, P. Ruffieux, R. Jaafar, M. Bieri, T. Braun, S. Blankenburg, M. Muoth, A. P. Seitsonen, M. Saleh, X. Feng, K. Müllen, and R. Fasel, *Nature* **466**, 470 (2010).
- <sup>26</sup>T. Shimizu, J. Haruyama, D. C. Marcano, D. V. Kosynkin, J. M. Tour, K. Hirose, and K. Suenaga, *Nat. Nanotechnol.* **6**, 45 (2011).
- <sup>27</sup>C. Tao, L. Jiao, O. V. Yazyev, Y.-C. Chen, J. Feng, X. Zhang, R. B. Capaz, J. M. Tour, A. Zettl, S. G. Louie, H. Dai, and M. F. Crommie, *Nat. Phys.* **7**, 616 (2011).
- <sup>28</sup>L. Grill, M. Dyer, L. Laffrentz, M. Persson, M. V. Peters, and S. Hecht, *Nat. Nanotechnol.* **2**, 687 (2007).
- <sup>29</sup>J. Björk, S. Stafström, and F. Hanke, *J. Am. Chem. Soc.* **133**, 14884 (2011).
- <sup>30</sup>C. Bronner, F. Leyssner, S. Strelau, M. Utecht, P. Saalfrank, T. Klamroth, and P. Tegeder, *Phys. Rev. B* **86**, 085444 (2012).
- <sup>31</sup>S. Linden, D. Zhong, A. Timmer, N. Aghdassi, J. H. Franke, H. Zhang, X. Feng, K. Müllen, H. Fuchs, L. Chi, and H. Zacharias, *Phys. Rev. Lett.* **108**, 216801 (2012).
- <sup>32</sup>P. Ruffieux, J. Cai, N. C. Plumb, L. Patthey, D. Prezzi, A. Ferretti, E. Molinari, X. Feng, K. Müllen, C. A. Pignedoli, and R. Fasel, *ACS Nano* **6**, 6930 (2012).
- <sup>33</sup>H. Huang, D. Wei, J. Sun, S. L. Wong, Y. P. Feng, A. H. Castro Neto, and A. T. S. Wee, *Sci. Rep.* **2**, 983 (2012).
- <sup>34</sup>H. Petek and S. Ogawa, *Prog. Surf. Sci.* **56**, 239 (1997).
- <sup>35</sup>C. D. Lindstrom and X.-Y. Zhu, *Chem. Rev.* **106**, 4281 (2006).
- <sup>36</sup>X.-Y. Zhu, *Annu. Rev. Phys. Chem.* **53**, 221 (2002).
- <sup>37</sup>J. E. Johns, E. A. Muller, J. M. J. Frechet, and C. B. Harris, *J. Am. Chem. Soc.* **132**, 15720 (2010).
- <sup>38</sup>M. P. Steele, M. L. Blumenfeld, and O. L. A. Monti, *J. Chem. Phys.* **133**, 124701 (2010).
- <sup>39</sup>F. Leyssner, S. Hagen, L. Óvári, J. Dokić, P. Saalfrank, M. V. Peters, S. Hecht, T. Klamroth, and P. Tegeder, *J. Phys. Chem. C* **114**, 1231 (2010).
- <sup>40</sup>N. Armbrust, J. Güdde, P. Jakob, and U. Höfer, *Phys. Rev. Lett.* **108**, 056801 (2012).
- <sup>41</sup>C. Bronner, M. Schulze, S. Hagen, and P. Tegeder, *New J. Phys.* **14**, 043023 (2012).
- <sup>42</sup>E. Varene, I. Martin, and P. Tegeder, *J. Phys. Chem. Lett.* **2**, 252 (2011).
- <sup>43</sup>S. Hagen, Y. Luo, R. Haag, M. Wolf, and P. Tegeder, *New J. Phys.* **12**, 125022 (2010).
- <sup>44</sup>C. Bronner, S. Strelau, M. Gille, F. Brausse, A. Haase, S. Hecht, and P. Tegeder, *Angew. Chem. Int. Ed.* **52**, 4422 (2013).
- <sup>45</sup>M. J. Frisch, G. W. Trucks, H. B. Schlegel *et al.*, Gaussian 09, Revision A.02, Gaussian Inc., Wallingford, CT, 2009.
- <sup>46</sup>C. Adamo and V. Barone, *J. Chem. Phys.* **110**, 6158 (1999).
- <sup>47</sup>T. Yanai, D. P. Tew, and N. C. Handy, *Chem. Phys. Lett.* **393**, 51 (2004).
- <sup>48</sup>M. Koch, F. Ample, C. Joachim, and L. Grill, *Nat. Nanotechnol.* **7**, 713 (2012).
- <sup>49</sup>L. Talirz, H. Söde, J. Cai, P. Ruffieux, S. Blankenburg, R. Jafaar, R. Berger, X. Feng, K. Müllen, D. Passerone, R. Fasel, and C. A. Pignedoli, *J. Am. Chem. Soc.* **135**, 2060 (2013).